Quantifying the Wave Energy Resource and Farm Siting Opportunities for Western Canada

Bryson Robertson[a*], Clayton Hiles[b], Ewelina Luzko[a], Bradley Buckham[a]

[*] *Corresponding Author, bryson@uvic.ca*

[a] *University of Victoria, Mechanical Engineering, PO Box 1700 STN CSC, Victoria, BC, V8W 3P6, Canada, +1(250)472-4065*

[b] *Cascadia Coast Research, 26 Bastion Square, Third Floor – Barnes House, Victoria, BC, V8W 1H9, Canada, +1(250)298-5055*

Abstract

Global wave energy inventories have shown that the West Coast of Canada possesses one of the most energetic wave climates in the world, with average annual wave energy transports of 40-50 kW/m occurring at the continental shelf. With this energetic climate there is an opportunity to generate significant quantities of electricity from renewable source through the use of wave energy conversion (WEC) technologies. However, a highly detailed, a priori understanding of both the temporal and spatial distribution of wave characteristics is paramount to the sustainable development of the wave energy opportunity in Western Canada. Such resource characterization informs on-going marine resource planning, educates policy advisors, and helps drive design studies of optimum WEC device physical sizing, PTO design and predicted annual power production.

To quantify the gross wave energy resource along the west coast of Vancouver Island, and hence the feasibility of deploying wave energy conversion technologies, a detailed Simulating WAves Nearshore (SWAN) numerical wave propagation model was developed. The SWAN model encompasses 410 000km^2 and covers 1500 km of the western Canadian coastline. The unstructured computational grid contains over 60 000 nodes and resolution is optimized by water depth and proximity to areas of high wave energy transport. The SWAN model hindcasts wave conditions along the West Coast for the 10 year period from 2004 to 2013, at a 3 hour time resolution over all 60 000 nodes. Independent validation of the SWAN model indicates a 0.92 correlation coefficient for significant wave heights and 0.80 for average wave periods.

The validated results from this hindcast model have enabled the characterization of the wave climate on the West Coast of Coast of Canada at an unprecedented level of detail. By analysing the gross wave resource data the data through the lens of optimum WEC operating conditions, novel methods allow for the filtering of the wave resource database to identify high priority WEC farm deployment locations. Using generic WEC performance metrics, theoretical wave farm outputs can be synthesized over a multiple year time scale. These theoretical wave farm power predictions are of paramount importance to both electrical utilities and policy makers. Armed with quantitative measures for future wave power plants, utilities will be able to determine the ability for the current electrical grid accept this renewable source of power, while policy developers will finally be able to bring clarity to the actual power producing potential for WEC farms.

Finally, this new understanding of the wave climate provides a more complete picture of the opportunity for WEC development in the region and will act as an industry enabler by providing developers access to detailed, validated wave data up-front without the need for significant investment.

Keywords: Wave Energy Resource Assessment, Wave Energy Converters, SWAN model, Power Integration, WEC Farms.

Notation:

The following symbols and abbreviations are used in this paper:

B = bias

d = directionality coefficient

E_{rms} = root mean square error

f_i = bin centre frequency corresponding to the i^{th} frequency band

g = gravity

J = omnidirectional wave energy transport

J_θ = directionally resolved wave energy transport

γ = JONSWAP peak-enhancement factor

ρ = seawater density

θ_i = wave direction for i^{th} frequency band

ϵ_0 = spectral width

H_{mo} = significant wave height

m_n = n^{th} wave spectral moment

r = correlation

S_i = variance density in the i^{th} frequency band

T_e = energy period

T_p = peak period

T_{avg} = average period

WEC = wave energy converter

WCWI = West Coast Wave Initiative

ECMWF= European Centre for Medium Range Weather Forecasts

COAMPS= Coupled Ocean Atmosphere Mesoscale Prediction System

CFSR = Climate Forecast System Reanalysis

NARR = North American Regional Reanalysis

GFS = Global Forecast System

NCEP = National Centres for Environmental Prediction

1 Introduction and Objectives

Global wave energy inventories have shown that the West Coast of Canada possesses one of the most energetic wave climates in the world, with average annual wave energy transports of 40-50 kW/m occurring at the continental shelf. With this energetic climate there is an opportunity to generate significant quantities of electricity from renewable source through the use of wave energy conversion (WEC) technologies. However, despite this large natural resource, progress within the wave energy conversion industry in Canada has been slow. This lack of strategic development has been hampered by a distinct lack of quantitative data on both the raw wave energy transport resource, and the potential electrical power generation from WEC farms. Through the use of highly resolved numerical wave modelling and knowledge of generic WEC dynamics, this study aims to fill these gaps in order to provide electrical utilities and policy makers the necessary information to determine to benefits, opportunities and costs associated with the development of a WEC industry in Canada.

In order to provide highly resolved raw wave energy transport data, including both the spatial and temporal variability, numerical hindcasts of wave conditions are utilized. Large-scale physics-based wave propagation models have been in operation since the 1960s, and undergo continuous revision to improve performance and extend the regions over which they can be applied [33-37]. The most commonly used models for wave resource assessments include Simulating WAves Nearshore (SWAN (SWAN, 2006)), Wave Watch III (WW3 (García-Medina et al., 2014)) and WAve Model (WAM). For the current study, a 10 year SWAN model hindcast and numerous wave measurement buoys are utilized.

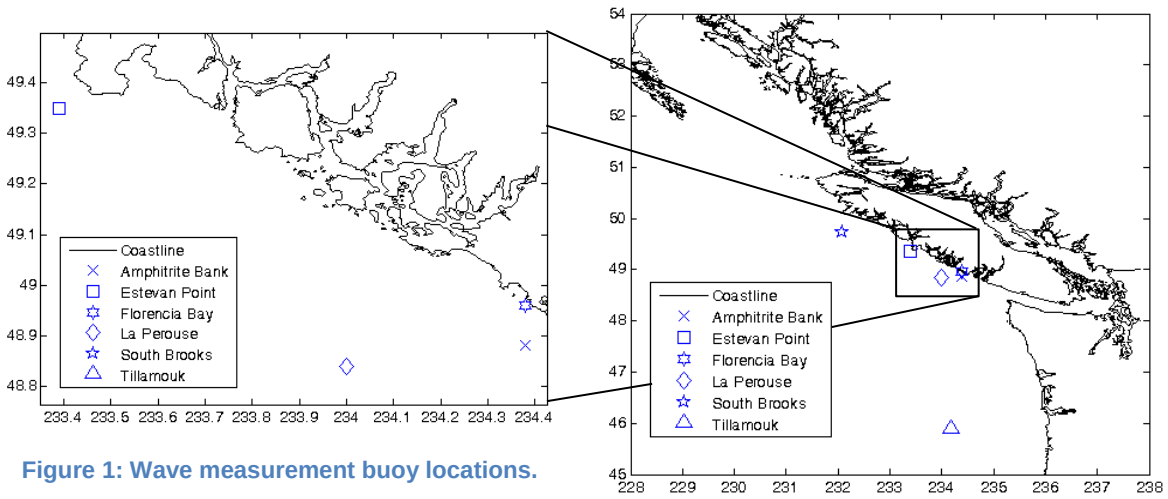

Figure 1: Wave measurement buoy locations.

The West Coast Wave Initiative (WCWI), within the Institute for Integrated Energy Systems at the University of Victoria, maintains both a series of buoys along the west coast of Vancouver Island and a highly resolved SWAN model for this region. Table 1 provides data on depth, time span, and location for each of the WCWI wave measurement buoys, as well as other relevant buoys operated by Environment Canada (EC) and National Ocean and Atmospheric Administration (NOAA). Figure 1 provides a map of the buoy locations. Utilizing the highly resolved 10 year SWAN hindcast, the spatial and temporal characteristics of wave climate along the west coast of Canada are quantified and validated against the wave measurement buoys.

Table 1: Wave buoy information

Location	Source	Depth	Starting Date	Resolution	Latitude	Longitude
Amphitrite Bank	WCWI	43 m	4/19/2013	Hourly	48.88 N	125.62 W
Estevan Point	WCWI	42 m	4/23/2013	Hourly	49.35 N	126.61 W
Florencia Bay	WCWI	25 m	6/1/2013	Hourly	48.96 N	125.62 W
La Perouse	EC	73 m	11/22/1988	Hourly	48.84 N	126.00 W
South Brooks	EC	2040 m	5/5/1994	Hourly	49.74 N	127.93 W
Tillamouk	NOAA	2289 m	11/10/2004	Hourly	45.89 N	125.82 W

The highly resolved resource data provides the necessary foundation for the estimation of electrical power production from wave farms. Given that metrics detailing WEC performance, such a performance matrices, are still evolving, this study utilizes generic WEC metrics for device performance in order to provide initial power production time-series predictions. This study provides a framework for future WEC device manufacturers and project developers to provide the necessary highly resolved wave power production estimates that will be required by regulatory and governmental agencies.

In Section 2 below, the resource assessment methodology is detailed. This includes details on a boundary condition sensitivity study and an independent model validation exercise completed using WCWI wave buoys. Section 3 provides the high resolution view of the wave resource metrics for Amphitrite Bank, as suggested by the International Electrotechnical Commission (IEC) Technical Committee 114 (IEC, 2014). Section 4 provides a framework for the wave farm location selection process and detailed information about the electrical power production from each wave farm site considered. Section 4 also presents the generic metrics used to quantify WEC performance.

Section 5 provides concluding remarks and recommendations for future work.

2 Resource Assessment Methodology

A variety of large scale global wind and wave model results are publically available for use in wave resource assessments, or as non-stationary boundary conditions for highly resolved regional model applications. For this study, the SWAN model is used. SWAN is a third generation phase-averaged Eulerian numerical wave model, designed to simulate the propagation of waves in shallow near-shore areas (Cornett and Zhang, 2008). The evolution of the wave spectrum is calculated by solving the action balance equation. The wave action density (N) is presented in Eq. (4) and evolves as a function of time (t), distance in the Cartesian coordinates (x,y), the shifting of relative frequency due to variation in depths and currents (σ), and depth and current induced refraction (ϑ). C_g denotes the wave action propagation speed in (x, y, σ, θ) space while S denotes the combined source and sink terms (Holthuijsen, 2008).

$$\partial N/\partial t + \partial C_{g,x}/\partial x + \partial C_{g,y}/\partial y + \partial C_{g,\sigma}/\partial \sigma + \partial C_{g,\theta}/\partial \theta = S/\sigma \quad (1)$$

where

$$S = S_{in} + S_{nl} + S_{wc} + S_{bf} + S_{br} \quad (2)$$

In deep water, the three major components of S are the input by wind (S_{IN}), nonlinear wave-wave interactions (S_{NL}) and wave dissipation through white-capping (S_{WC}). In shallow water, S includes the effects of bottom friction (S_{BF}) and shoaling-induced breaking (S_{BR}). Further documentation on the base SWAN model is available online(SWAN, 2006).

2.1 Characteristic Quantities for Wave Energy Conversion

The wave variance density spectrum is typically used to provide a detailed quantification of ocean surface waves. The SWAN model and wave buoys both record the full frequency domain wave spectrum, through numerical techniques and analysis of time-series accelerations respectively. Using the spectrums from either the SWAN model or the buoy data, the wave spectral moments are calculated from the variance density spectrum (S_i), according to Eq. (3):

$$m_n = \sum_i f_i^n S_i \, \Delta f_i \tag{3}$$

Initially, the peak wave period (T_p), which represents the frequency band with the highest variance in the spectrum, was extracted for each hour. Next, the energy period (T_{avg}) and significant wave height (H_{m0}) for each spectrum were calculated using Eq. (4) and Eq. (5) below:

$$T_{avg} = \sqrt[2]{m_0/m_2} \tag{4}$$

$$H_{m0} = 4.004\sqrt{m_0} \tag{5}$$

In addition to significant wave height and wave period parameters, the omnidirectional wave energy transport (J), described by Eq. (6), is commonly output:

$$J = \rho g \sum_i C_{g,i} S_{i,j} \Delta f_i \Delta \theta_j \tag{6}$$

However, when investigating potential wave energy development sites, a series of additional wave sea state characteristics have been proposed to account for the frequency and direction distribution of energy within the wave spectrum. These are included in the Draft Specification for Wave Resource Assessment by the International Electrotechnical Commission (IEC) Technical Committee 114 (IEC, 2014). These additional parameters include the spectra width (ϵ_o), which is defined by:

$$\epsilon_0 = \sqrt{\frac{m_o m_2}{m_1^2} - 1} \tag{7}$$

ϵ_o values of 0 indicate that a single frequency (regular) wave, while large values of ϵ_o indicate a greater spread of energy across the frequency spectrum. Additionally, acknowledging that many WEC designs have a directional operating principal, knowledge of the direction and magnitude of the maximum directionally resolved wave energy transport (J_θ) is important. The directionally resolved wave energy transport is calculated by:

$$J_\theta = \rho g \sum_{i,j} S_{i,j} \Delta f_i \Delta \theta_j \cos(\theta - \theta_j)\delta \quad \delta = \begin{cases} 0 & if \ \cos(\theta - \theta_j) < 0 \\ 1 & if \cos(\theta - \theta_j) \geq 0 \end{cases} \tag{8}$$

From Eq. (8), it is possible to quantify both the maximum directionally resolved wave energy transport (J_{θ_J}) and associated direction (θ_J). In addition, the directionality co-efficient (*d*) describes the ratio of directionally resolved wave energy transport and the bulk total wave energy transport (*J*):

$$d = \frac{J_{\theta_J}}{J} \tag{9}$$

As *d* approaches 1, the associated directionally resolved wave energy transport spectrum narrows along the direction axis and the directional spreading is lowered. For detailed explanations of these additional parameters, see Lenee-Bluhm *et al.(2011a)*.

2.2 SWAN Model Development

The performance of SWAN model results are directly correlated to input boundary conditions, wave propagation numerics and the computational grid resolution. Hence, it is imperative to determine which large scale models provide the best performance as boundary conditions for the area of interest. This completed through direct quantitative comparison against EC and NOAA wave measurement buoys. The EC and NOAA buoys were used to determine the optimum SWAN model set-up, while the WCWI buoys were used to independently validate the SWAN model performance.

Within the domain of interest, the bathymetric depth ranges from approximately 1,000 m at the continental shelf to approximately 5m at the surf line. In order to ensure computational efficiency and improve resolution of nonlinear wave effects in shallower water, an unstructured computational grid was used. In deeper water, large grid spacing is sufficient, while in shallow water the smaller grid spacing is required to capture the wave transformations that occur due to interaction with the ocean floor. Grid spacing for the SWAN computational was specified proportional to water depth, and reduces below 20m for locations within significant bathymetric features. For this region, the wave propagation numerics were studied in detail by Robertson et al. (2013) and kept at the suggested values.

2.2.1 Wind Boundary Conditions

There are numerous global wind models which provide the necessary data coverage to allow for use as a SWAN wind boundary condition. Through a detailed comparison of 17 global model outputs, compared on the basis of time resolution, spatial resolution, data period and ease of access, it was determined that the COAMPS model from FNMOC, the Climate Forecast System Reanalysis (CFSR), the North American Regional Reanalysis (NARR) and the Global Forecast System (GFS), all from the National Centres for Environmental Prediction (NCEP), provided the necessary resolution and warranted further investigation.

Table 2: Wind boundary condition performance

La Perouse	COAMPS	CFSR	NARR	GFS
B	0.03	-0.93	-1.03	-0.85
E_{rms}	2.15	2.24	2.32	1.77
r	0.82	0.84	0.83	0.91
South Brooks				
B	-0.14	0.79	-1.05	-0.54
E_{rms}	2.23	2.06	2.41	1.75
r	0.84	0.90	0.84	0.90

To quantify the performance of each wind model, the model results were compared against directly recorded wind measurements from the wave measurement buoys at La Perouse Bank and South Brooks (see Figure 1). As shown in Table 2, the COAMPS and GFS models provide an excellent combination of low bias (B), low root-mean-square error (E_{rms}) high correlation (r) values.

2.2.2 Wave Boundary Conditions

The preferred wave boundary conditions for the SWAN model are fully directional wave buoy measurements, yet geographically appropriate measurements are not currently available for Vancouver Island. Fortunately, numerical models outputs from the NOAA's WW3 model and the European Centre

for Medium Range Weather Forecasts WAM models were available. NOAA's WW3 model outputs directional spectrums at the Environment Canada NOMAD buoys, offshore Vancouver Island, while the ECMWF WAM model stores full directional spectra at thousands of locations globally.

To determine which wave boundary condition resulted in superior performance, SWAN model runs for both wave boundary conditions, using the COAMPS wind model, were conducted. As shown in Table 3, the ECMWF boundary condition result in significant wave height (H_{mo}) and peak wave period (T_p) results which consistently correlate higher with buoy measurements than results using NOAA ww3 boundary conditions.

Table 3: Wave boundary condition performance

		South Brooks		La Perouse		Tillamouk	
		ECMWF WAM	NOAA WW3	ECMWF WAM	NOAA WW3	ECMWF WAM	NOAA WW3
H_{mo}	B	-0.35	-0.20	-0.09	0.00	-0.04	0.24
	E_{rms}	0.67	0.69	0.49	0.57	0.14	0.16
	r	0.91	0.89	0.94	0.92	0.94	0.93
T_p	B	0.21	0.22	0.16	0.12	0.48	0.20
	E_{rms}	1.85	1.97	0.13	0.15	1.93	2.08
	r	0.67	0.63	0.72	0.64	0.63	0.67

2.2.3 Combined Wind / Wave Boundary Conditions

In order to validate the final SWAN model and determine which wind boundary condition resulted in the best representation of the measured seastate, an additional series of SWAN runs were completed using the ECMWF wave boundary condition with the COAMPS and GFS wind fields. As shown in Table 4, the ECMWF/COAMPS model combination provided slightly better correlation and lower bias values when compared against the ECMWF/GFS combination. It is expected that the improved correlation could be due to the increased spatial resolution of the COAMPS model (0.2°) when compared to the GFS model (0.5°).

Table 4: SWAN model validation

		South Brooks		La Perouse		Tillamouk	
ECMWF w/		COAMPS	GFS	COAMPS	GFS	COAMPS	GFS
H_{mo}	B	-0.352	-0.508	-0.094	-0.204	-0.038	-0.074
	E_{rms}	0.674	0.823	0.492	0.557	0.141	0.504
	r	0.913	0.898	0.940	0.940	0.938	0.942
T_p	B	0.206	0.402	0.158	0.197	0.485	0.505
	E_{rms}	1.852	1.830	0.135	1.647	1.928	1.942
	r	0.672	0.680	0.719	0.705	0.630	0.624

In conclusion, prospective boundary condition data sources for the SWAN model were filtered to determine best predictive performance. The boundary condition selection was determined by testing the SWAN model performance, with each combination of boundary conditions, against wave buoy measurements. This processes identified that the ECMWF wave and COAMPS wind boundary conditions resulted in the best performance in the SWAN model.

2.3 SWAN Model Validation

As previously noted, the SWAN model development and boundary condition choice was determined through detailed analysis of performance against EC and NOAA wave buoys. The WCWI wave measurement buoys, noted in Table 1, were used to independently validate the SWAN model performance. The model was validated by comparing H_{mo}, T_p and T_{avg} from the SWAN hindcasts against the measured values at the WCWI buoy sites. Table 3 presents the annual mean performance for the decade long hindcast against the WCWI wave buoys of Amphitrite Bank, Estevan Point and Florencia Bay.

		Amphitrite Bank	Estevan Point	Florencia Bay
H_{mo}	B	0.062	0.030	0.075
	E_{rms}	0.340	0.413	0.280
	r	0.939	0.884	0.937
T_p	B	1.010	0.608	0.692
	E_{rms}	2.985	3.020	3.284
	r	0.576	0.555	0.552
T_{avg}	B	0.077	-0.185	-0.010
	E_{rms}	0.746	0.788	0.668
	r	0.821	0.815	0.767

As Table 3 demonstrates, the SWAN model estimates H_S with a high degree of accuracy at all three locations. At Amphitrite Bank, the correlation is 0.94, while Estevan Point and Florencia Bay reports correlations of 0.88 and 0.94 respectively. Similarly, the bias ranges from as little as 3 centimeters at Estevan Point to 8 cms at Florencia Bay. Given the unstable nature of peak periods, the lower correlation values for peak wave are expected. As a result, the average wave period is included to better indicate the performance of the model. Given that the average wave period uses the entire spectrum, rather than just the peak, it provides a better indication of the spectral performance of the model. The correlations are much higher for the average wave period at 0.77 to 0.82. Additionally, the average wave period bias is less than 1/10 second on average.

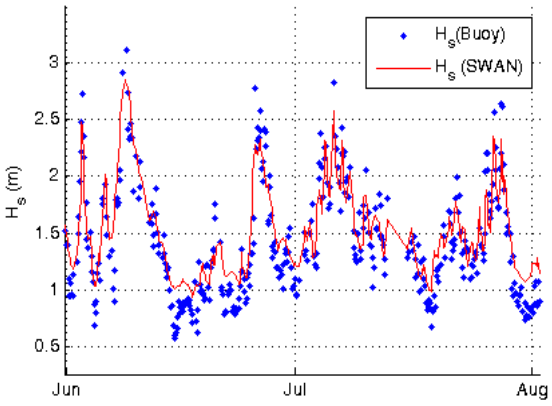

Figure 2: H_{mo} SWAN validation at Estevan Point

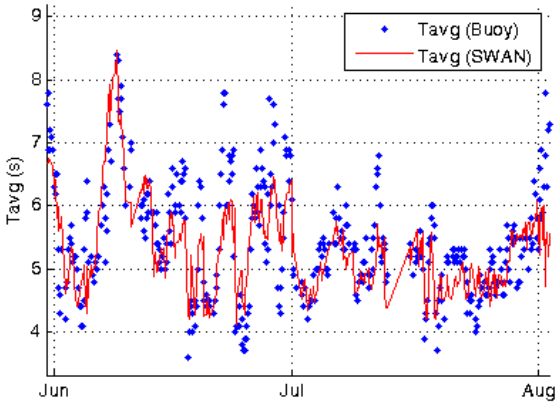

Figure 3: T_{avg} SWAN validation at Estevan Point

Shown in Figure 2 and Figure 3 are the actual and simulated values for H_{mo} and T_{avg} at Estevan Point, over a period of two months. The measured buoy data is more volatile, with more frequent outliers, while the SWAN simulation is smoother. Physics models are inherently limited by the accuracy and

resolution of forcing wind fields, and are generally unable to reproduce short-lived extreme wave events. However, the SWAN model is able to reproduce both the seasonality in the wave height and much of the short-term variability (Robertson et al., 2013). Given the significant correlation between the SWAN model and the three independent WCWI buoys, it was determined that the performance of the SWAN had been validated and could be used to investigate longer term trends.

3 West Coast Wave Climate Characteristics

To gain a higher fidelity understanding of the wave energy transport and associated sea states off the west coast of Vancouver Island, the SWAN model hindcast was run for 10 years from 2004 until 2013. The annual and monthly mean wave parameters were calculated to determine the spatial and depth variability of wave characteristics. These time averaged characteristics reveal a great deal when attempting to identify optimum wave farm analyzing the suitability of a single location, or the whole west coast, for future wave energy conversion activities.

Figure 4 gives the mean annual wave energy transport $\bar{J}$ for the years 2005 - 2010 over the entire computational domain. Like previous course-resolution studies (Cornett, 2006; Cornett, 2008; Pontes et al., 1996), $\bar{J}$ is approximately 45 kW/m along the continental shelf. The mean annual H_{m0} plot follows a very similar pattern to $\bar{J}$ and shows a correspondingly steady decrease in the annual mean wave height as the seafloor depth decreases. Significant spatial variation in $\bar{J}$ and H_{m0} close to shore due to depth induced refraction and localised diffraction creates areas of energy concentration and dilution. The inclusion of diffractive effects is most important in locations protected from direct swell propagation, such as coastal inlets and harbours.

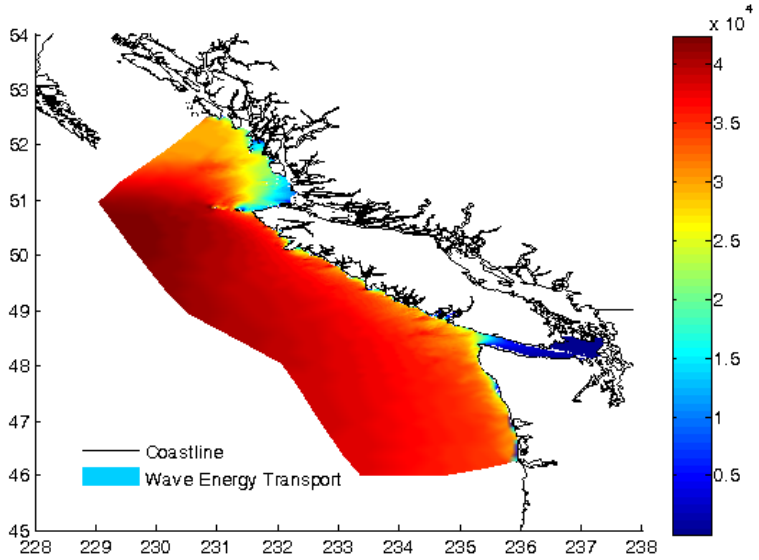

Figure 4: Mean annual wave energy transport off Vancouver Island (W/m)

To illustrate the annual variability within the wave resource, mean monthly characteristics were extracted from the Amphitrite Bank buoy location. The Amphitrite Bank is approximately 7 km offshore and has previously been identified as a possible site for wave energy conversion (Cornett and Zhang, 2008; Kim et al., 2012). The bathymetric bank concentrates wave energy through refraction and results in high mean wave energy transport values close to shore. The predicted mean annual $\bar{J}$ for the 2003 to 2014 period is 34.56 kW/m at the Amphitrite buoy.

Figure 5 illustrates the variation in monthly mean directional wave energy transport (J_θ) values, while Figure 6 shows the variation in the directionality co-efficient . The mean +/- one standard deviation, 10th, 50th and 90th percentiles of J_θ are additionally plotted. Focusing on Figure 5, a seasonal shift in the directional wave energy transport is immediately evident, with monthly mean values of 50 kW/m occurring during winter and only 6.5 kW/m occurring during the calmer summer months. The low summer values are directly related to the decrease in the significant wave heights during this period.

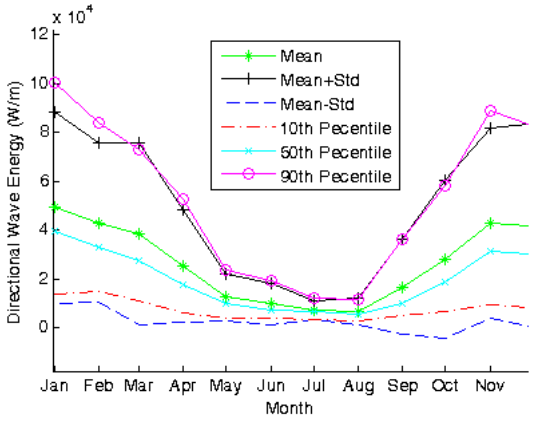

Figure 5: Monthly variation in J_θ at Amphitrite Bank

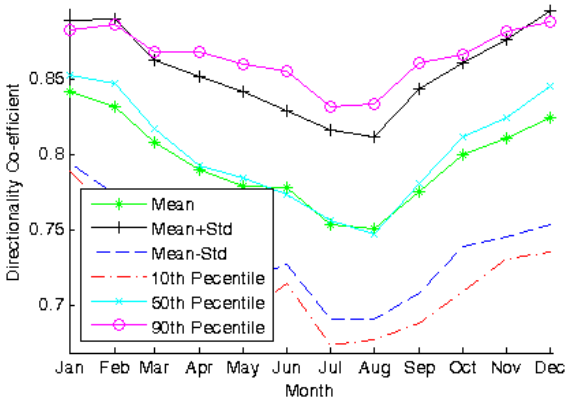

Figure 6: Monthly variation in d at Amphitrite Bank

In Figure 6, the mean directionality coefficient (d) also varies considerably throughout the year. Over the winter months, mean d values reach 0.84 yet fall to 0.75 during the summer. This is due to the dominance of significant ground swell wave systems during the winter while summer months are defined by predominant localised wind seas.

Finally, histograms of wave height and energy period are often used to convey the wave climate characteristics in locations of interest. Shown in Figure 7, the mean annual frequency and energy transport characteristics of individual wave height and period combinations for the 2004 – 2013 period. The wave height is organized in 0.5m bins while the wave period is discretized by 1 second intervals. The frequency in number of hours per year is illustrated by the numerical values in each discrete combination, while the percentage of total wave energy transport is indicated by the contour colour ramp.

Immediately evident is the fact that the sea state of maximum occurrence does not correspond to the sea state with the highest percentage annualized wave energy transport. In Figure 7, the most commonly occurring wave state is H_{m0} = 1.25m at T_e = 8.50 seconds, occurring for 782 hours annually, while the sea state which features the highest energy transport is H_{m0} = 2.75m at T_e = 10.5 seconds (~ 5.7 %). However, this seastate only occurs 366 hours per year. These findings agree with similar findings (Hiles et al., 2013; Lenee-Bluhm et al., 2011b; Robertson et al., 2013).

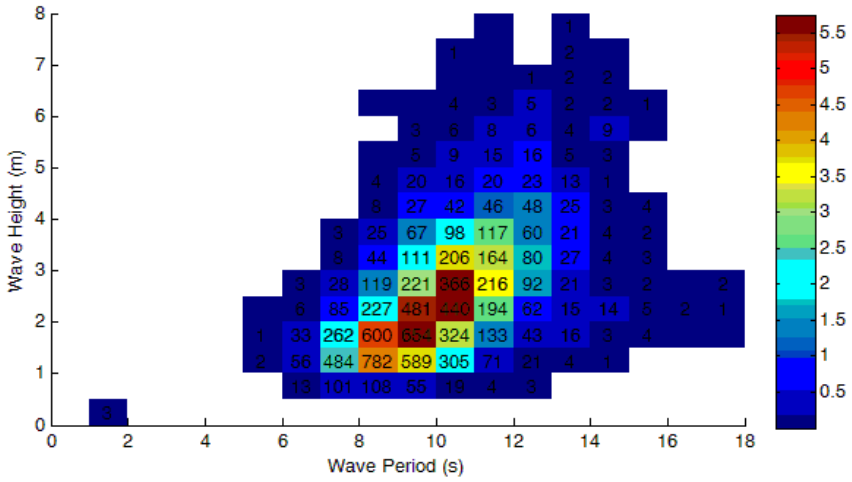

Figure 7: Histogram showing the probability and energy distribution at the Amphitrite buoy location.

4 Wave Farm Site and Power Production Characteristics

Initial investigations on potential wave farm deployment sites were determined through detailed analyses of the wave resource potential, distance from the site to shore and the proximity to existing electrical infrastructure. For this research, investigations were conducted to determine the best locations for 10 theoretical wave farms off the west coast of Vancouver Island.

To identify locations as potential site for future wave farms, it is necessary to filter the spatially extensive, raw wave resource data presented above. As part of this process, a number of assumptions about distance from shore, deployment depth and WEC device performance were required. These assumptions will require constant revision as the requirements from WEC developers and electrical utilities become clearer. Given that the study goal was to provide a WEC architecture independent assessment of possible power production, specific WEC performance curves purposely omitted and generic performance estimates were used.

4.1 WEC Farm and Device Characteristics

Initially, all sites beyond 15 km from shore were eliminated from the area of interest. This is due to the high costs associated with procurement and laying seafloor electrical cables. The added operating and maintenance costs associated with deep water sites make these sites increasingly unattractive. Within this distance constraint, the research area shown in Figure 4 is significantly reduced to the areas shown in Figure 8 and Figure 9. To display the localized differences in wave energy transport, the Hesquiaht Peninsula is isolated in Figure 9. As shown, the western tip features an area of high wave energy transport (~ 40 kW/m) while the eastern bay displays lower energy transport values (< 5 kW/m). These differences illustrate the need of highly resolved nearshore wave models (like SWAN) in order to ensure siting in the most active wave climates.

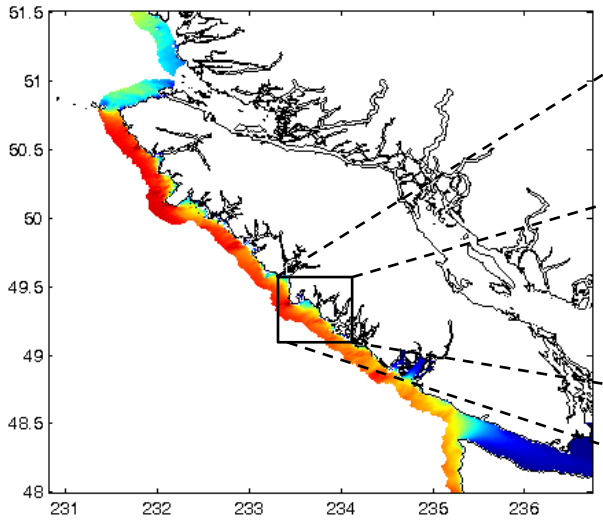

Figure 8: Wave Energy Transport - 15km Region

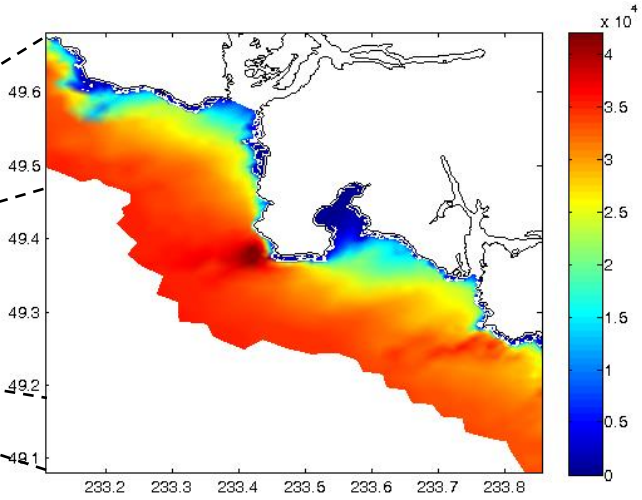

Figure 9: Wave Energy Transport - 15km Estevan Point

Next, in order to predict 10 potential wave farm locations within the 15km swath, the annual wave energy transport values associated with each computational grid node were ranked by magnitude. By plotting the top 15th percentile, 30th percentile and 50th percentile of annual wave energy transport values, areas with higher J_{mean} values were easily identified and noted.

By overlaying all the sites, identified through the percentile analysis, with a map of the current electrical transmission grid from BC Hydro (Hydro, 2014), ten reasonably distributed, high energy nodes were chosen. The black squares in Figure 10 and Figure 11 illustrate the spatial distribution of the potential sites. Table 5 presents the latitude and longitude for each potential wave farm. Note the wave farm number is determined by the mean wave energy transport values from the SWAN model rather than by geographic location. The Estevan Point buoy and the Amphitrite Bank buoys are located in Farms 4 and 10 respectively.

Each potential wave farm location was assumed to cover 16 km^2 (4 km X 4 km) and is centered around the node identified through the detailed percentile analysis above. In order to quantify the theoretical wave power production from the sites identified, each 16 km^2 area populated with an installation of 50, 100 and 250 devices.

Table 5: Wave farm locations and power production characteristics

Farm:	# 1	# 2	# 3	# 4	# 5	# 6	# 7	# 8	# 9	# 10	Units
Latitude	233.40	232.81	232.48	232.10	231.96	231.79	231.80	231.65	232.04	234.35	Deg
Longitude	49.37	49.78	49.92	50.10	50.19	50.53	50.51	50.63	50.14	48.84	Deg
Power Production	142.0	141.5	141.1	130.4	142.7	135.9	126.3	131.7	131.3	135.5	GWhr
Std Deviation	14.61	14.46	14.34	13.48	14.45	13.72	12.99	13.83	13.7	13.97	MW
Minimum	0.896	0.894	0.945	0.834	0.607	0.752	0.757	0.419	0.731	0.481	MW
Maximum	50	50	50	50	50	50	50	50	50	50	MW

Exact coordinates for each WEC were determined by assuming each WEC featured a characteristic 20 m diameter and, to ensure non-destructive interference and maintenance tolerance, each device potential location was spaced 200m apart. Each WEC was assumed to have a maximum rated power of 200 kW and featured 10% energy conversion efficiency. As a result, the maximum power production for each farm was 10, 20 or 50 MW depending on the number of installed devices.

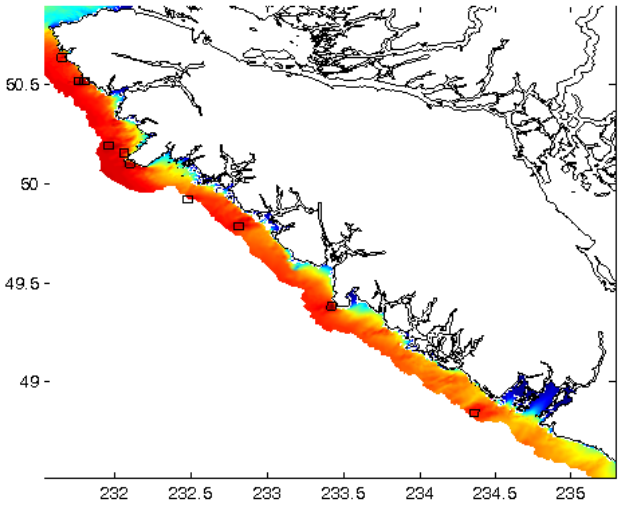

Figure 10: Potential Wave Farm Locations

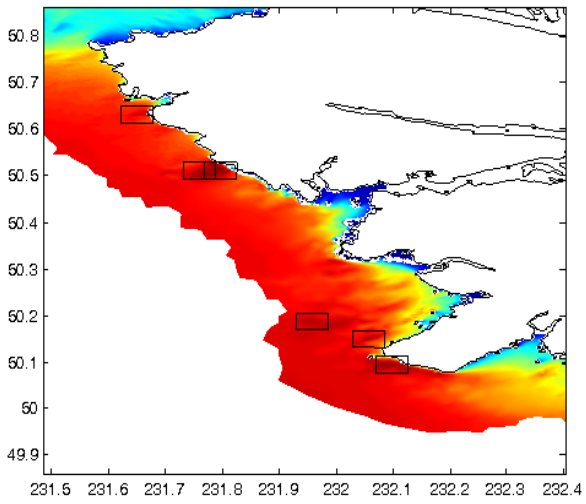

Figure 11: Potential Wave Farm Locations – Northern Vancouver Island

4.2 Wave Farm Electrical Output

To provide an initial estimate of the power production from WEC farms off the west coast of Canada, it is necessary to ensure that the wave conditions used as inputs to the farm simulations are representative of the long term wave climate. Knowing that the wave conditions for individual characteristic hours are not going to be consistent year to year, the representative year of wave conditions was chosen by ensuring the annual wave energy transport for the representative year was consistent with the mean annual wave energy transport from the 10 year hindcast. 2008 was shown have the smallest variation from the 10 year mean wave energy transport conditions.

Estimates of wave farm electrical power outputs were then calculated by using Eq. (10):

$$P_{elec} = \sum_{i=i}^{n} J_{wave} * W_{wec} * \eta_{wec} \quad (10)$$

where n is the number of WEC devices, J_{wave} is the wave energy transport, W_{wec} is the characteristic width (20m) and η_{wec} is the WEC efficiency (10%). However, if P_{elec} > 200kW*n, the power output was limited to 200n.

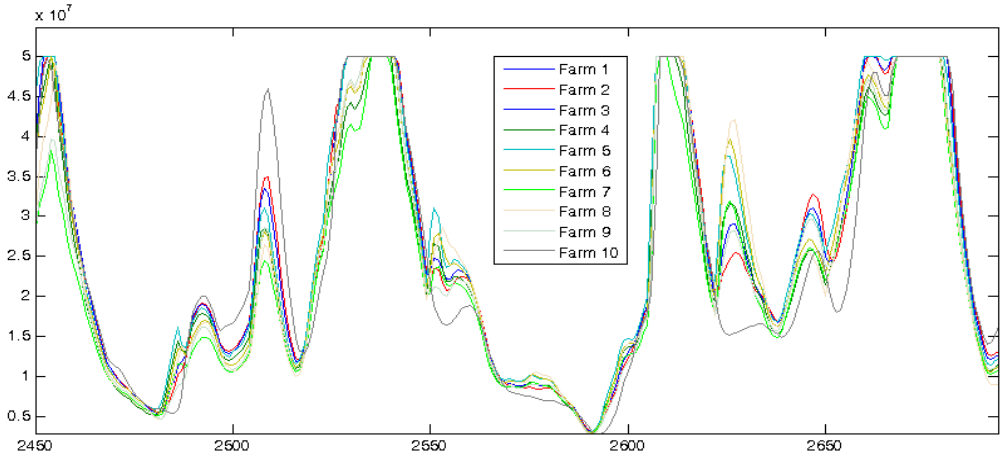

Figure 12: Wave Farm Electrical Power Output (250 WEC's with 200kW rating)

Table 5 provides overview characteristics of the power produced from each wave farm during 2008. The mean annual power production varies between 142 GWhrs and 126 GWhrs. Figure 12 presents the total power output from each of the 10 wave farms over 10 days in November 2008. Each wave farm for this simulation consisted of 250 units at 200 kW rated power, and hence the maximum rated power for each farm being 5 MW. It is noted that the power output from individual WEC farms follow a similar power production trend due to the direct link to wave conditions off Vancouver Island.

However, as illustrated in Figure 13 and Figure 14, the relative magnitude of the electrical power outputs do vary across the 10 proposed wave farms as a result of the farm spatial spreading and incident wave conditions. For example, the improved production peak for Farm 10 in Figure 13 results from a swell impacting the southern portion of Vancouver Island, yet not affecting the northern portion of the island. This directional effect of the incoming wave regime results in an approximate 90% variation in the power output across the 10 farms. The power production increase at 2625 hours in Figure 14 indicates the opposite phenomenon.

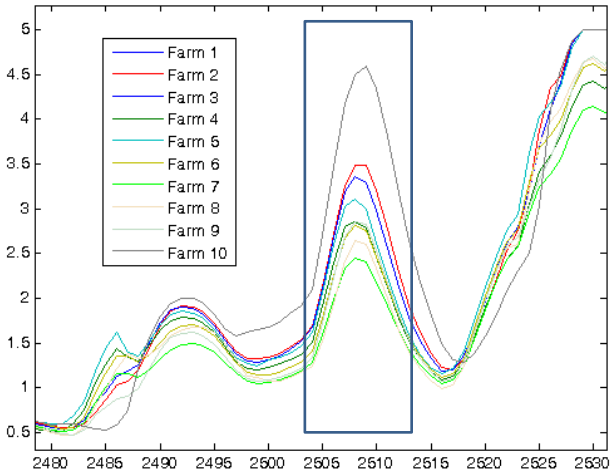

Figure 13: Power Production Estimate (SW swell)

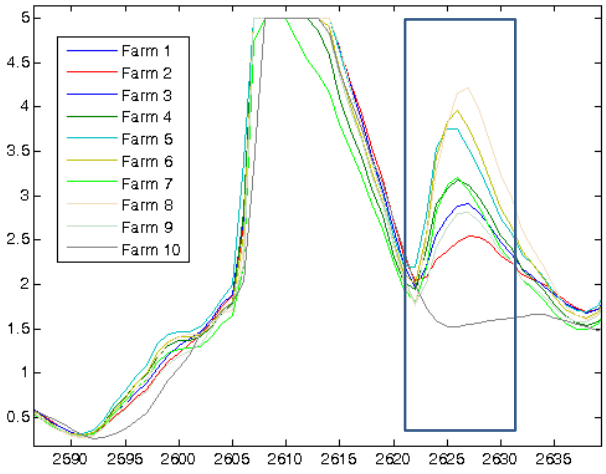

Figure 14: Power Production Estimate (NW swell)

Without detailed knowledge of the electrical grid performance, it cannot be determined if this variation in farm output is of benefit or detriment to maintaining the power grid in British Columbia. Regardless, these power production simulations are of paramount importance to the development of a wave energy industry within Canada. Without them, utilities and policy makers will be unable to make informed decisions on both the benefit and/or detriment to the development of a wave energy conversion industry in Canada.

5 Conclusions and Recommendations

Global wave energy inventories have shown that the West Coast of Canada possesses one of the most energetic wave climates in the world, with average annual wave energy transports of 40-50 kW/m occurring at the continental shelf. With this energetic climate there is an opportunity to generate significant quantities of electricity from renewable source through the use of wave energy conversion (WEC) technologies.
To quantify the gross wave energy resource along the west coast of Vancouver Island, and hence the feasibility of deploying wave energy conversion technologies, a detailed Simulating WAves Nearshore (SWAN) numerical wave propagation model was developed. The SWAN model encompasses 410 000km^2 and

covers 1500 km of western Canadian coastline. The SWAN model hindcasts wave conditions along the West Coast for the 10 year period from 2004 to 2013, at a 3 hour time resolution over all 60 000 nodes.

Sensitivity studies investigating the performance of numerous global wind and wave models provided quantitative evidence to determine that the combination of ECMWF wave and COAMPS wind boundary conditions results in the best correlation against three EC and NOAA wave measurement buoys. Independent validation of the SWAN model indicated an impressive 0.92 correlation coefficient for significant wave heights and 0.80 for average wave periods.

Amphitrite Bank, off Ucluelet British Columbia, has often been noted as an area of interest for wave energy conversion development. Detailed analysis of SWAN model results at Amphitrite Bank provided details on the frequency, magnitude and directional distribution of the wave energy resource throughout a typical year. The mean monthly directional wave energy transport and directionality coefficients were shown to be vary between 6 - 50 kW/m and 0.75 – 0.84 respectively. Higher values of wave energy transport and directionality were measured during winter swell events, while lower values were recorded during summer wind sea conditions. Annual mean bivariate distributions for Amphitrite Bank illustrate both the hours of occurrences of each sea state and the percentage contribution for each sea state to the total annual energy transport. As shown in previous resource assessments worldwide (Hiles et al., 2013; Lenee-Bluhm et al., 2011b; Robertson et al., 2013), the most frequent sea state does not coincide with the most energetic. The most common sea state at Amphitrite Bank sea states was H_{m0} = 1.25m and T_e = 8.5 seconds (782 hours). However, waves of H_{m0} = 2.75m and T_e = 10.5 seconds feature approximately 40% more annual wave energy transport but only occur 366 hours per year.

Using the SWAN model results and a percentile analysis of all annual wave energy transport values, within 15 km of shore and close to current electrical grid infrastructure, 10 prospective wave farm locations were identified. Applying architecture independent WEC performance metrics, power production time series for wave farms with rated capacities of 50 MW, 20 MW and 10 MW were synthesized. Basic analysis of the resulting production time series illustrated the variation in the production from different farms due to their inherent spatial distribution and the historical wave climate. Finally policy makers and electrical utilities have the quantitative data required to bring clarity to the value proposition for wave energy conversion. The production of these theoretical wave farm power production estimates for the British Columbia is a significant step forward towards determining the benefits, opportunities and detriments associated with producing ocean renewable energy.

Acknowledgements

This work was funded by Natural Resources Canada, the Pacific Institute of Climate Solutions and the Natural Sciences and Research Council of Canada.

References

Cornett, A., 2006. Inventory of canada's marine renewable energy resources. CHC-TR-041, National Research Council - Canadian Hydraulics Centre, Ottawa, K1A 0R6, Canada.

Cornett, A. and Zhang, J., 2008. Nearshore wave energy resources, western vancouver island, b.C. CHC-TR-51, Canadian Hydraulics Centre.

Cornett, A.M., 2008. A global wave energy resource assessment. proceedings of the 18th international offshore and polar engineering conference, Vancouver, Canada, p.^pp.

García-Medina, G., Özkan-Haller, H.T. and Ruggiero, P., 2014. Wave resource assessment in oregon and southwest washington, USA. Renewable Energy, 64: 203-214.

Hiles, C., Buckham, B., Wild, P. and Robertson, B., 2013. Ocean renewable wave energy resources near hot springs cove, canada. Renewable Energy, 71: 598-608.

Holthuijsen, L.H. (Editor), 2008. Waves in oceanic and coastal waters. Cambridge Press.

Hydro, B., 2014. Bulk provincial transmission system.

IEC, 2014. International electrotechnical commission tc 114: Marine energy - wave, tidal and other water current converters.

Kim, C.-K. et al., 2012. Catching the right wave: Evaluating wave energy resources and potential compatibility with existing marine and coastal uses. PloS one, 7(11): e47598.

Lenee-Bluhm, P., Paasch, R. and Özkan-Haller, H.T., 2011a. Characterizing the wave energy resource of the us pacific northwest. Renewable Energy, 36(8): 2106-2119.

Lenee-Bluhm, P., Paasch, R. and Ozkan, H.T., 2011b. Characterizing the wave energy resource of the us pacific northwest. Renewable Energy, 36: 2106-2119.

Pontes, M.T. et al., 1996. An atlas of the wave-energy resource in europe. Journal of Offshore Mechanics and Arctic Engineering, 118(4): 307-309.

Robertson, B., Hiles, C. and Buckham, B., 2013. Characterizing the nearshore wave energy resource on the west coast of vancouver island. Renewable Energy, 71: 665-678.

SWAN, t., 2006. Swan technicial manual. Delft University of Technology, P.O. Box 5048 2600 GA Delft The Netherlands.